A Bi-directional, Isolated, Single-Stage, DAB-based AC-DC converter with Open-loop Power Factor Correction and Other Advanced Features

Gysler Castelino, Kaushik Basu, Nathan Weise and Ned Mohan

***Abstract*—In this paper, a control method for an AC-DC converter is proposed that simultaneously has the following features: a) galvanic isolation b) bi-directional power flow, c) Zero Current Switching (ZCS) for the primary side switches and Zero Voltage Switching (ZVS) turn-on for the secondary side, d) linear power relationship for easy control implementation, e) unity power factor with open-loop control and f) single-stage power conversion. It is thoroughly analyzed by first assuming it to be a DC-DC converter in a push-pull topology and then extending the results to analyze an AC-DC converter. The conclusions of the analysis are confirmed by simulations.**

I. Introduction

AC-DC power conversion that requires galvanic isolation can be bulky due to presence of a low frequency transformer. With the help of power electronics, this low frequency transformer can be replaced by a compact high frequency transformer. The switching frequency is however limited by the device stress, and switching losses [1]. Hence converters having soft-switching characteristics are being explored. A review of AC-DC converters using high frequency transformers is given in [2]. These converters have good power factor however they have unidirectional power flow and have multiple stages.

Dual Active Bridge Converters (DABC) are a class of high frequency transformer-isolated converters that have inherent qualities of soft switching, low device stress and small filter requirements. These make them suitable for applications requiring high power density. DABC was introduced in [3], [4]; in this converter, two square-wave voltages are phase shift modulated (PSM) to control the power flow using the leakage inductance of the transformer. When the input and output voltages vary widely, the soft switching range of PSM DABC is limited. New modulations methods, where one of the converters is duty-ratio modulated were proposed to extend this soft switching range [5]. In [6], [7] and [8] Trapezoidal and Triangular current modulation are introduced and analyzed. Triangular current mode modulation is used when the input and output voltages are different; this strategy results in maximum ZVS/ZCS at the cost of high rms currents [9]. In trapezoidal current modulation, low rms currents are obtained in the transformer and higher power transfer is possible compared to triangular current modulation. The inner mode and outer mode of operation of DABC are explored in [10] and [11]. It is possible to obtain ZCS in the low voltage side in the 'inner mode' of operation. Triangular current mode modulation is a special case of the 'inner mode' of operation.

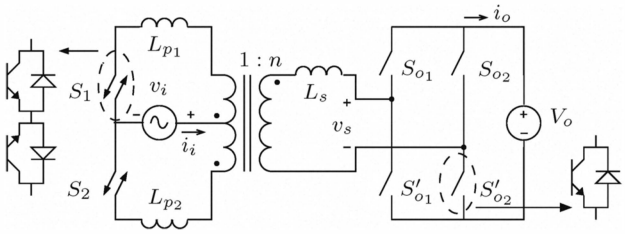

Fig. 1. AC-DC converter

A comprehensive analysis of all the modes of operation of a DABC is given in [12].

The design and control of a multi-stage single-phase AC-DC DABC with unity power factor is given in [13]. The drawback of this converter is that it lacks bi-directional capability and is not single-stage. The dual-active bridge principle is applied to the AC-DC converter in [14], [15]. In [14] and [15] the AC-DC converter operates in inner as well as outer mode of operation in order to obtain maximum soft switching. A topology with bi-directional functionality as well as a unity power factor on the utility side is proposed in [16]. The control of these AC-DC converters is complicated as it is non-linear.

In this paper, a control method for a AC-DC converter shown in Fig. 1 is proposed that simultaneously has the following features: a) galvanic isolation, b) bi-directional power flow, c) ZCS for the primary side switches and ZVS turn-on for the secondary side, d) linear power relationship for easy control implementation, and e) unity power factor under open-loop control and f) single-stage power conversion. In order to analyze a single-phase AC-DC converter, first, the 'inner mode' of operation for a DC-DC DABC with the primary switches in push-pull topology is analyzed in subsection II-A. This analysis is extended to single-phase AC-DC converter in subsection II-B. In section III, the simulation results in SABER are compared with the theoretical analysis.

II. Analysis of the proposed AC-DC converter with advanced features

An AC-DC Dual Active Bridge Converter (DABC) with the primary side in push-pull configuration is shown in Fig. 1. An AC voltage source $v_i = \hat{V}_i \sin(\omega t)$, where $\omega = 2\pi f$ is connected to the primary of a three-winding high-frequency transformer and a DC voltage source V_o is connected to the secondary of the high frequency transformer through a H-bridge inverter. The turns ratio of one half of the primary

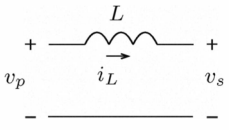

Fig. 2. Equivalent circuit of the converter system from the secondary side

winding to the secondary winding of the transformer is 1 : n. In the following analysis, it is assumed that $V_o \geq n\hat{V}_i$. The leakage inductances of the two primary windings are L_{p_1} and L_{p_2} and that of the secondary winding is L_s. The primary side switches S_1 and S_2 are four-quadrant. They are switched at 50% duty-ratio in a complementary way at a switching frequency of $f_s(=\frac{1}{T_s})$. If the leakage inductance of the two primary windings are identical, $L_{p_1} = L_{p_2} = L_p$, and the magnetizing current is neglected, the equivalent circuit of the converter system seen from the secondary side of the transformer is shown in Fig. 2 where, $L = n^2L_p + L_s$. The voltage v_p is $+nv_i$ when S_1 is ON and is $-nv_i$ when S_2 is ON. In one switching cycle, the net volt-sec applied to the transformer is zero; thus, the flux in the transformer core is balanced in the modulation technique described below. The secondary side switches S'_{o_1} and S'_{o_2} are switched complementary to S_{o_1} and S_{o_2} respectively. The voltage v_s can be controlled to be $+V_o$, $-V_o$ or 0.

A. Analysis of DC-DC Converter

In a DC-DC DABC, the input voltage in Fig. 1 is constant at V_i. The switches S_1 and S_2 can be two-quadrant. In the 'inner mode' of operation, the secondary side converter is pulse-width modulated with a duty-ratio given by (1). A phase shift of $\delta\frac{T_s}{2}$ is introduced between the voltages v_p and v_s to obtain power transfer (Fig.3 (a)). In this mode, the absolute value of δ is limited by (2) [12]. This modulation technique ensures that the average voltage applied across the inductor is zero every $T_s/2$ and the switches S_1 and S_2 are switched at zero current, thus reducing the switching losses considerably. An added advantage is that a snubber circuit is no longer necessary for these switches. The inductor current i_L, i_o and i_i are shown in Fig. 3 (c), (d) and (e) respectively.

$$d = \frac{nV_i}{V_o} \tag{1}$$

$$0 \leq |\delta| \leq (1-d)\frac{1}{2} \tag{2}$$

The secondary side converter can be modulated by two switching strategies; in the first case (Fig. 3 (a)), the zero voltage is applied by turning on S'_{o_1} and S'_{o_2}. In the second method (Fig. 3 (b)), the zero voltage is applied either by S_{o_1} and S_{o_2} or by S'_{o_1} and S'_{o_2}; this method has an advantage that the secondary side pulses are square wave. A dead-time is introduced between the transition of switches in the same leg. The switches in the secondary side turn on under ZVS condition as anti-parallel diodes are conducting when these switches are turned on. This condition is true for any direction

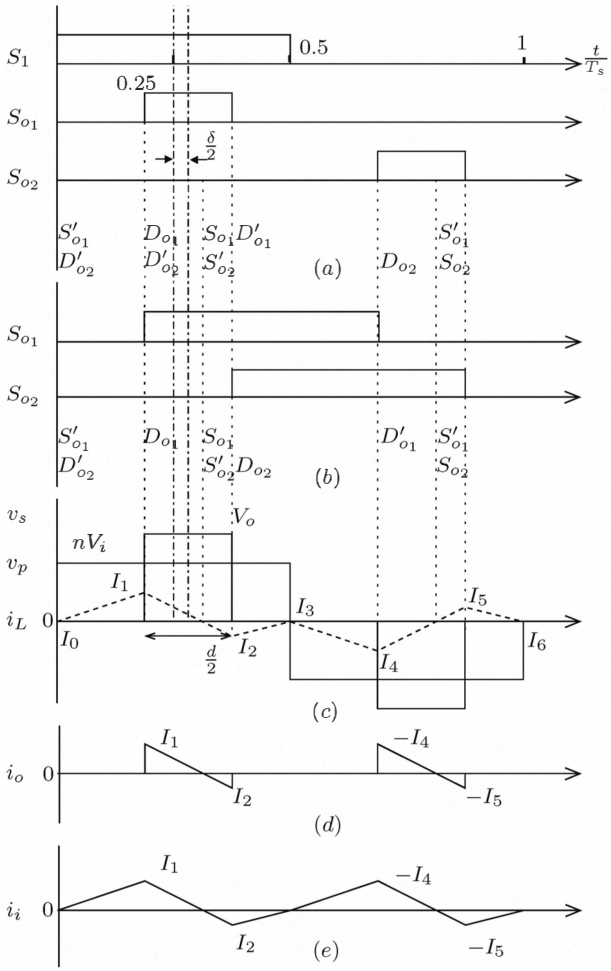

Fig. 3. Switching waveforms for DC-DC converter

of power flow. In case the current is not zero every half cycle, all the secondary side switches are turned off, so that the diodes and V_o form a clamp circuit that brings the current down to zero. Now, S_1 and S_2 can be safely switched.

The voltage, current and power bases are selected as (3). The average power supplied is calculated to be (4). A maximum power of 0.233 pu can be transferred using this converter when $d = 2/3$. Due to the constraints on the value of δ, the power transferred in the inner mode of operation is lesser than a PSM DABC [3](0.523 pu at d=2/3).

$$\left.\begin{aligned} V_{base} &= V_o \\ I_{base} &= \frac{V_o}{2\pi f_s L} \\ P_{base} &= \frac{V_o^2}{2\pi f_s L} \end{aligned}\right\} \tag{3}$$

$$\begin{aligned} P_{io} &= \delta d\frac{nV_iV_o}{2Lf_s} = \delta d^2\frac{V_o^2}{2Lf_s} \\ &= \delta d^2\pi \qquad \cdots \text{in pu} \end{aligned} \tag{4}$$

The per unit rms currents in the transformer are calculated to be (5) and (6). The primary and secondary rms voltages

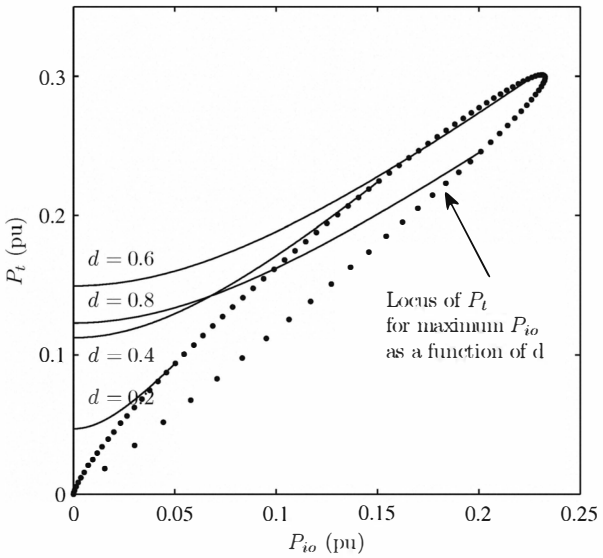

Fig. 4. DC-DC Converter: P_t Vs P_{io}

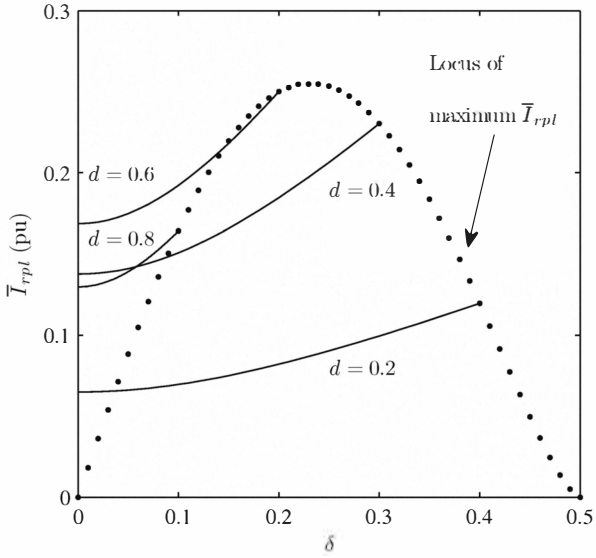

Fig. 5. DC-DC Converter: $\overline{I}_{rpl}$ Vs δ

are calculated in (7) and (8) respectively. Using these values the transformer per unit VA can be calculated as (9). The per-unit values of P_t are plotted as a function of P_{io} in Fig. 4. A transformer per unit VA of $P_t = 0.299$pu is required to transfer the maximum power of 0.233pu, which corresponds to a transformer utilization (P_{io}/P_t) of 0.779, This is higher than the transformer utilization (0.636) for maximum power transfer at the diode bridge boundary for topology B in [3].

$$\overline{I}_{L_s} = K\sqrt{(1-2d+d^2+12\delta^2)d^2} \tag{5}$$

where, $K = \dfrac{2\pi}{4\sqrt{3}}$

$$\overline{I}_{L_{p_1}} = \overline{I}_{L_{p_2}} = \frac{\overline{I}_{L_s}}{\sqrt{2}} \tag{6}$$

$$\overline{V}_p = \frac{d}{\sqrt{2}} \tag{7}$$

$$\overline{V}_s = \sqrt{d} \tag{8}$$

$$P_t = \frac{1}{2}[2\overline{V}_p\overline{I}_{L_p} + \overline{V}_s\overline{I}_{L_s}] = \frac{1}{2}(d+\sqrt{d})\overline{I}_{L_s} \tag{9}$$

The size of the dc-side filter capacitor is a function of the rms ripple current through it. The per-unit value of the rms ripple current through the dc capacitor, $\overline{I}_{rpl}$ is given by (11). In Fig. 5, the worst case ripple equals 0.256 pu at δ of 0.23 (d=0.54).

$$\overline{I}_o = K\sqrt{(1-2d+d^2+12\delta^2)d^3} \tag{10}$$

$$\overline{I}_{rpl} = K\sqrt{(1-2d+d^2+12\delta^2(1-d))d^3} \tag{11}$$

B. Analysis of Single-Phase AC-DC Converter

Consider a single-phase phase AC-DC converter in Fig. 1. As $f_s \gg f$, in one switching cycle, the input voltage can be approximated as a DC voltage. In the positive half cycle, the ZCS conditions for the primary side switches are satisfied when the output side converter is modulated with a duty ratio of (12). In the negative half cycle, the pulses for S_{o_1} and S_{o_2} are interchanged. The duty ratio d of the secondary side converter varies with time, hence the maximum value of δ also varies with time (13). Selecting a constant value of δ ensures unity power factor on the AC side. For a given value of m, $|\delta|$ is constrained by (14).

$$d(t) = m|\sin(\omega t)| \qquad \cdots \; m = \frac{n\hat{V}_i}{V_o} \tag{12}$$

$$0 \le |\delta| \le \frac{1}{2}(1-d(t)) \tag{13}$$

$$0 \le |\delta| \le \frac{1}{2}(1-m) \tag{14}$$

The instantaneous power transferred (15) is obtained by replacing V_i and d in (4) by $\hat{V}_i\sin(\omega t)$ and (12) respectively. From the definition of input power, the switching-cycle averaged input current ($\tilde{i}_i(t)$) can be calculated as (16). Under open-loop control, the switching-cycle averaged input current is in phase with the input voltage and unity power factor is obtained. The average power, P_{avg} is calculated by integrating the instantaneous power over one fundamental cycle of the input voltage. The following inferences are made about P_{avg}: 1) The power flow has a linear relationship to δ this simplifies the control strategy where power flow can be bi-directional by changing the sign of δ. 2) As m increases, the range of δ reduces. 3) No power can be transferred when $V_o = n\hat{V}_i$. 4) The locus of maximum power that can be transferred is

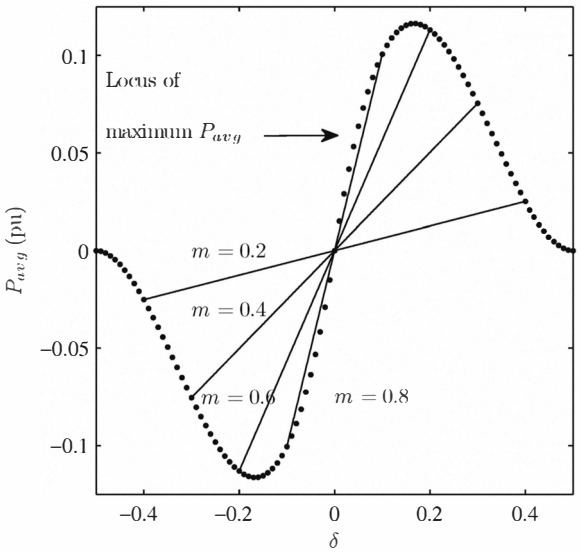

Fig. 6. AC-DC Converter: P_{avg} Vs δ

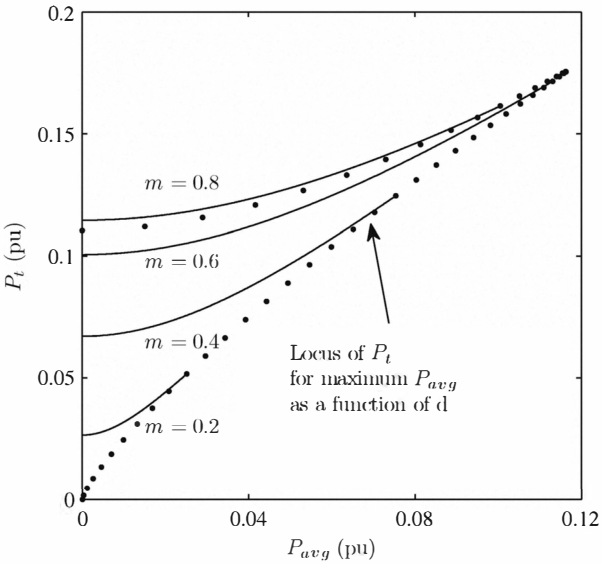

Fig. 7. AC-DC Converter: P_t Vs P_{avg}

plotted by the dotted curve in Fig. 6. The maximum value of P_{avg} (0.116 pu) occurs when $m = 2/3$.

$$P(t) = \frac{\delta n^2 \hat{V_i}^2}{2Lf_s} \sin^2(\omega t) \tag{15}$$

$$\tilde{i}_i(t) = \frac{P(t)}{V_i(t)} = \frac{\delta n^2 \hat{V_i}}{2Lf_s} \sin(\omega t) \tag{16}$$

$$P_{avg} = \frac{1}{2\pi} \int_0^{2\pi} P(\omega t) d(\omega t) \tag{17}$$

$$P_{avg} = \delta n^2 \frac{\hat{V_i}^2 V_o}{4Lf_s} = \delta m^2 \frac{V_o^2}{4Lf_s} = \frac{1}{2}\delta m^2 \pi \quad \cdots \text{in pu} \tag{18}$$

The rms currents in the transformer windings over one switching period are a function of $d(t)$ and are given by (5) and (6). The equation for the rms currents through the transformer windings over one cycle of the input voltage (given by (19) and (20)) can be found by integrating the the square of (5) and (6) and determining root of the mean. The rms values for the primary and secondary voltages are given by (21) and (22) respectively. The transformer per unit VA rating is calculated by (23). The per-unit values of P_t are plotted as a function of P_{avg} in Fig. 7. The dotted curve marks the locus of maximum VA for the transformer for different values of P_{avg}. To transfer the maximum power (0.116 pu), the transformer VA required is 0.176, resulting in a transformer utilization of 0.663. This is the maximum utilization of the transformer.

$$\overline{I}_{L_s} = K' m \sqrt{9m^2\pi - 64m + 12\pi(1 + 12\delta^2)} \tag{19}$$

where, $K' = 0.1044$

$$\overline{I}_{L_{p_1}} = \overline{I}_{L_{p_2}} = \frac{\overline{I}_{L_s}}{\sqrt{2}} \tag{20}$$

$$\overline{V}_p = \frac{m}{2} \tag{21}$$

$$\overline{V}_s = \sqrt{\frac{2m}{\pi}} \tag{22}$$

$$P_t = \frac{1}{2}[2\overline{V}_p \overline{I}_{L_p} + \overline{V}_s \overline{I}_{L_s}] = \frac{1}{2}\left(\frac{m}{\sqrt{2}} + \sqrt{\frac{2m}{\pi}}\right)\overline{I}_{L_s} \tag{23}$$

The rms values for i_o and ripple current in the dc-capacitor given by (24) and (25) are calculated from (10) and (11) respectively. The per-unit values of the dc-capacitor current ripple is plotted for selected values of m as a function of δ in Fig. 8. The maximum value for $\overline{I}_{rpl}$ (0.185 pu) occurs when δ is 0.21(m=0.58) at a power transfer of 0.111 pu.

$$\overline{I}_o = K'' \sqrt{m^3(64m^2 - 45m\pi + 80(1 + 12\delta^2))} \tag{24}$$

$$\overline{I}_{rpl} = K'' \sqrt{m^3(64m^2 - 45m\pi - 270\pi\delta^2 m + 80 + 960\delta^2)} \tag{25}$$

where, $K'' = 0.0661$

III. Simulation results

The DC-DC converter in Fig. 1 is simulated in SABER. The converter parameters are listed in Table I. The waveforms for

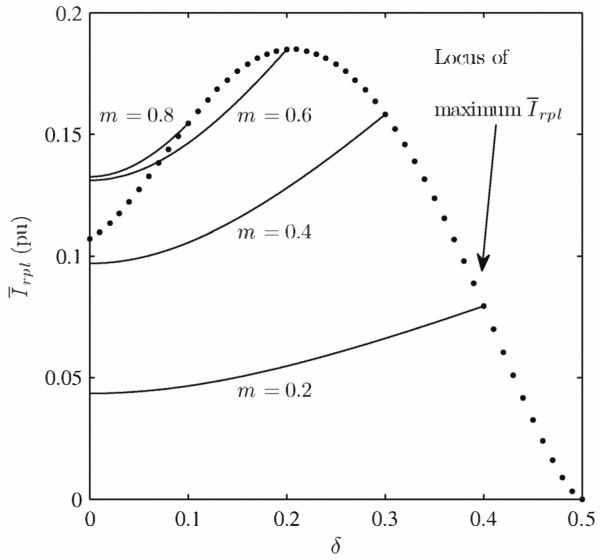

Fig. 8. AC-DC Converter: $\overline{I}_{rpl}$ Vs δ

TABLE I
SIMULATION PARAMETERS

$V_i = \hat{V}_i$	40V
V_o	200V
f_s ,f	5kHz , 60Hz
$L_{p_1} = L_{p_2} = L_s$	50μH
turns-ratio	1:1:1
δ	0.1

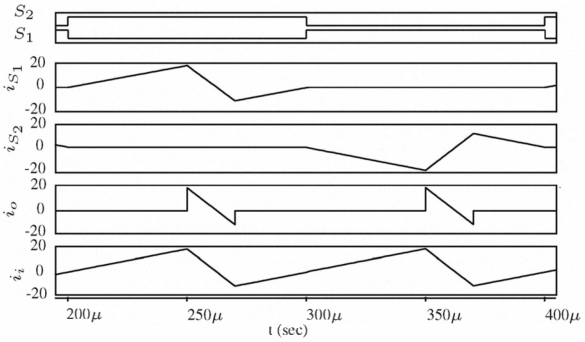

Fig. 9. Simulation Result: DC-DC Converter

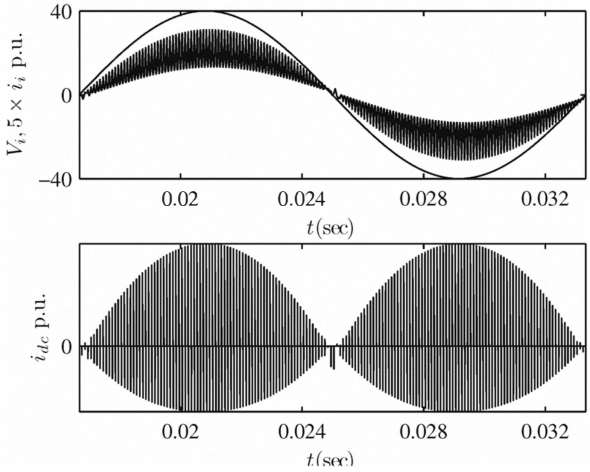

Fig. 10. Simulation Result: Single-Phase AC-DC

the current through S_1 and S_2 as well as the input and output currents are shown in Fig. 9. As these currents are zero at the transition of S_1 or S_2, zero switching for primary switches is confirmed.

A single-phase AC-DC converter having parameters listed in Table I is also simulated in SABER. In Fig. 10, the input voltage and filtered input current are in phase with each other, indicating that a unity power factor of operation is obtained. The calculated and simulated values for P_{io}, I_i, I_o and I_{cap} for both DC-DC and AC-DC converters match closely as listed in Table II.

IV. CONCLUSION

In this paper, a modulation technique for a DABC-based AC-DC converter is proposed that results in several beneficial features simultaneously. The salient features are single-stage power conversion, bi-directional power flow, open-loop unity power factor of operation, ZCS in the primary side under all loading conditions, ZVS turn on for all secondary side switches and high power density. Single-stage power conversion is an improvement over conventional multi-stage AC-DC converters with bulky low frequency transformers. Along with isolation, the high-frequency transformer blocks dc-injection to the AC-side and provides voltage transformation. The bi-directional property of this converter makes is especially attractive for distributed battery resources. By operating in the 'inner mode' with constant phase shift, open-loop unity power factor is obtained on the AC-side. The linear relationship between power and δ makes it easy to control. Zero Current Switching (ZCS) on the low voltage (high-current) side will lead to reduction in switching losses and improved efficiency. The switching frequency can also be increased, thus reducing the size of the magnetic components considerably. However, this potential reduction in size needs to be evaluated in light of higher rms currents that result to achieve ZCS. It should be noted that in Fig. 1, a full bridge topology can be employed instead of a push-pull topology; hence a single primary winding can be used at the expense of twice the

TABLE II
COMPARISON OF SIMULATION AND CALCULATED VALUES

Parameter	Simulation (DC-DC)	Calculation (DC-DC)	Simulation (AC-DC)	Calculation (AC-DC)
P_{io}	158.81 W	160 W	79.51 W	80 W
$\overline{I}_i$(rms)	10.12 A	10.06 A	7.27 A	7.35 A
$\overline{I}_o$(rms)	4.53 A	4.50 A	2.96 A	3.01 A
$\overline{I}_{rpl}$(rms)	4.46 A	4.43 A	2.93 A	2.97A

number of switches on the primary side.

REFERENCES

[1] N. Mohan, T. Undeland, and W. Robbins, *Power Electronics: Converters, Applications, and Design*, 3rd ed., 2003, vol. 1.

[2] B. Singh, S. Singh, A. Chandra, and K. Al-Haddad, "Comprehensive study of single-phase ac-dc power factor corrected converters with high-frequency isolation," *Industrial Informatics, IEEE Transactions on*, vol. PP, no. 99, p. 1, 2011.

[3] R. De Doncker, D. Divan, and M. Kheraluwala, "A three-phase soft-switched high power density dc/dc converter for high power applications," in *Industry Applications Society Annual Meeting, 1988., Conference Record of the 1988 IEEE*, Oct. 1988, pp. 796 –805 vol.1.

[4] M. Kheraluwala, R. Gasgoigne, D. Divan, and E. Bauman, "Performance characterization of a high power dual active bridge dc/dc converter," in *Industry Applications Society Annual Meeting, 1990., Conference Record of the 1990 IEEE*, Oct. 1990, pp. 1267 –1273 vol.2.

[5] N. Schibli, "Dc-dc converters for two-quadrant operation with controlled output voltage," in *EPFL*, 1999.

[6] F. Krismer, J. Biela, and J. Kolar, "A comparative evaluation of isolated bi-directional dc/dc converters with wide input and output voltage range," in *Industry Applications Conference, 2005. Fourtieth IAS Annual Meeting. Conference Record of the 2005*, vol. 1, 2005, pp. 599 – 606 Vol. 1.

[7] F. Krismer, S. Round, and J. Kolar, "Performance optimization of a high current dual active bridge with a wide operating voltage range," in *Power Electronics Specialists Conference, 2006. PESC '06. 37th IEEE*, 2006, pp. 1 –7.

[8] G. Ortiz, J. Biela, D. Bortis, and J. Kolar, "1 megawatt, 20 khz, isolated, bidirectional 12kv to 1.2kv dc-dc converter for renewable energy applications," in *Power Electronics Conference (IPEC), 2010 International*, june 2010, pp. 3212 –3219.

[9] Y. Wang, S. de Haan, and J. Ferreira, "Optimal operating ranges of three modulation methods in dual active bridge converters," in *Power Electronics and Motion Control Conference, 2009. IPEMC '09. IEEE 6th International*, may 2009, pp. 1397 –1401.

[10] H. Tao, A. Kotsopoulos, J. Duarte, and M. Hendrix, "A soft-switched three-port bidirectional converter for fuel cell and supercapacitor applications," in *Power Electronics Specialists Conference, 2005. PESC '05. IEEE 36th*, 2005, pp. 2487 –2493.

[11] H. Tao, A. Kotsopoulos, and J. Duarte, "Transformer-coupled multiport zvs bidirectional dc-dc converter with wide input range," *Power Electronics, IEEE Transactions on*, vol. 23, no. 2, pp. 771 –781, 2008.

[12] A. K. Jain and R. Ayyanar, "Pwm control of dual active bridge: Comprehensive analysis and experimental verification," *Power Electronics, IEEE Transactions on*, 2010.

[13] M. Kheraluwala and R. De Doncker, "Single phase unity power factor control for dual active bridge converter," in *Industry Applications Society Annual Meeting, 1993., Conference Record of the 1993 IEEE*, Oct. 1993, pp. 909 –916 vol.2.

[14] K. Vangen, T. Melaa, and A. Adnanes, "Soft-switched high-frequency, high power dc/ac converter with igbt," in *Power Electronics Specialists Conference, 1992. PESC '92 Record., 23rd Annual IEEE*, jun-3 jul 1992, pp. 26 –33 vol.1.

[15] K. Vangen, T. Melaa, S. Bergsmark, and R. Nilsen, "Efficient high-frequency soft-switched power converter with signal processor control," in *Telecommunications Energy Conference, 1991. INTELEC '91., 13th International*, nov 1991, pp. 631 –639.

[16] N. Weise, K. Mohapatra, and N. Mohan, "Universal utility interface for plug-in hybrid electric vehicles with vehicle-to-grid functionality," in *Power and Energy Society General Meeting, 2010 IEEE*, 2010, pp. 1 –8.